

# Controllable non-Hermitian Qubit-Qubit Coupling in Superconducting Quantum Circuit

Hui Wang,<sup>1,2</sup> Yan-Jun Zhao,<sup>3</sup> and Xun-Wei Xu<sup>4</sup>

<sup>1</sup>*Inspur artificial intelligence research institute, Jinan, 250014, China*

<sup>2</sup>*Shandong Yunhai Guochuang Innovative Technology Co., Ltd., Jinan 250101, China*

<sup>3</sup>*Key Laboratory of Opto-electronic Technology, Ministry of Education, Beijing University of Technology, Beijing, 100124, China*

<sup>4</sup>*Key Laboratory of Low-Dimensional Quantum Structures and Quantum Control of Ministry of Education, Key Laboratory for Matter Microstructure and Function of Hunan Province, Department of Physics and Synergetic Innovation Center for Quantum Effects and Applications, Hunan Normal University, Changsha 410081, China*

(\*Electronic mail: xwxu@hunnu.edu.cn )

(\*Electronic mail: wanghuiPHY@126.com)

(Dated: 18 December 2024)

We propose a theoretical scheme to realize the controllable non-Hermitian qubit-qubit coupling by adding a high-loss resonator in tunable coupling superconducting quantum circuit. By changing the effective qubit-qubit coupling, phase and amplitude of resonator-qubit interaction, and the qubits' quantum states, we can continually tune the energy level attraction, position of EP (exceptional point), and the nonreciprocity in the non-Hermitian superconducting circuit. The EPs and non-reciprocity can affect the quantum states' evolutions and exchange efficiencies for two qubits in the non-Hermitian superconducting circuit. The controllable non-Hermitian and nonreciprocal interactions between two qubits provide a new insights and methods for exploring the unconventional quantum effects in superconducting quantum circuit.

## I. INTRODUCTION

Non-Hermitian system possesses complex energy spectrum, and the real and imaginary parts respectively label the energy levels and loss, while the starting and ending points of energy level degenerate points are known as the EPs (exceptional points)<sup>1-5</sup>. The non-Hermitian coupling is essentially dissipative type interaction which has been proposed to realize the entangled quantum states<sup>6-8</sup>. The system close to exceptional points contain rich unconventional physical effects, including the ultralow driving threshold chaos<sup>9</sup>, high sensitivity metrology<sup>10,11</sup>, high-dimensions skin effect<sup>12,13</sup>, chiral heat transport<sup>14</sup> and so on. The EP (exceptional point) have been studied in single ion system<sup>15,16</sup>, optical microcavity<sup>10,17-23</sup>, and optomechanical system<sup>24-27</sup>, magnonic system<sup>28-30</sup>, hybrid quantum system<sup>31</sup>, cavity magnonics<sup>24,32,33</sup>, single superconducting qubit<sup>34-36</sup>, and so on. Some theoretical work have studied the  $PT$ -symmetry in superconducting circuit with the single qubit coupling to the resonator<sup>37,38</sup>. However, it is still challenging to experimentally observe such non-Hermitian in multi-qubits superconducting circuit due to the difficulties in realizing controlled gain and loss.

Unlike the efforts to improve the gain and loss of superconducting resonator, we use a high-loss resonator to supply the effective non-Hermitian interactions between two qubits in tunable coupling superconducting circuit. The effective energy levels and damping rates of two qubits can be controlled by effective qubit-qubit coupling, phase and amplitude of qubit-resonator coupling, and the quantum state of qubits. Because of special parameter dependent relation in superconducting circuit, the energy levels attraction and positions of EPs are controllable. The non-reciprocal interactions between two qubits can also appear in non-Hermitian superconducting

quantum circuit, which can be used to develop the integrated unidirectional transmission devices including the microwave circulator and isolator.

The qubits' quantum state evolutions and states exchanges are also affected by the EPs which might be useful for the quick initialization of qubits and the tunable quantum gates. The Rabi oscillation periods of two non-reciprocal coupling qubits are different which can be measured with current experimental skills.

The paper is organized as follows: In Sec. II, we build the physical model of non-Hermitian superconducting circuit; In Sec. III, the energy level attractions and quantum state evolutions in non-Hermitian circuit are studied; In Sec. IV, we analyze the non-reciprocal coupling and quantum state exchange between two qubits. We finally summarize the results in Sec. V.

## II. PHYSICAL MODEL

As shown in Fig. 1, the system is formed by adding a high-loss resonator on the tunable coupling superconducting circuit consisting of two Xmon qubits and a transmon coupler. The transmon coupler can induce coherent interaction between two qubits, and the high-loss resonator supply the non-Hermitian interaction. The Xmon qubit is a modified version of transmon qubit, and the cross-type capacitance could suppress the sensitivity of the qubit to charge noises<sup>39,40</sup> and facilitate for design of superconducting quantum chip<sup>41</sup>. The total Hamiltonian for the superconducting circuit in Fig. 1 can be obtained as  $H = H_0 + H_{xy} + \sum_j H_{qc}^{(j)} + \sum_j H_{qr}^{(j)}$ , and the expressions of free Hamiltonian  $H_0$ , direct qubit-qubit interaction Hamiltonian  $H_{xy}$ , and coupler-qubit- $j$  interaction Hamil-

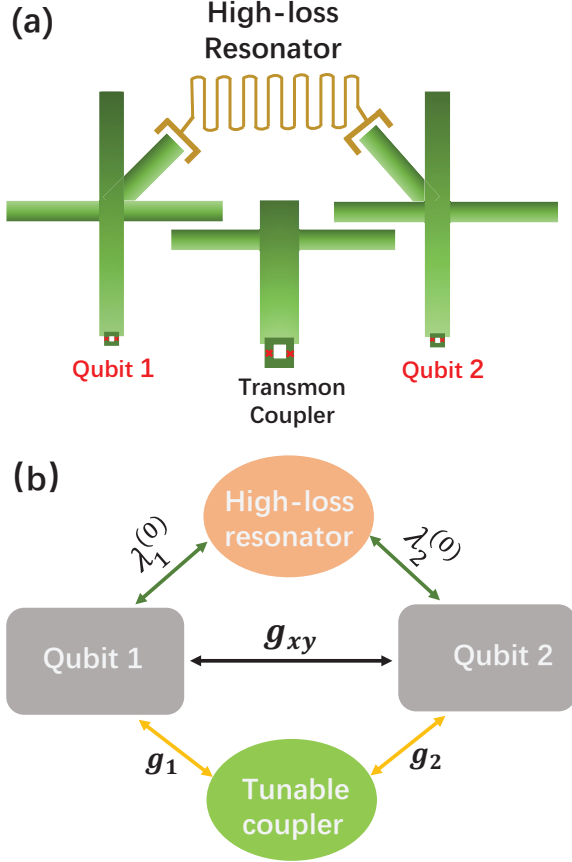


FIG. 1. (Color online) (a) Schematic diagram and (b) coupling scheme in superconducting quantum circuit. The circuit consisting of two Xmon qubits couple to a common transmon coupler and a common high-loss resonator.  $g_j$  and  $\lambda_j^{(0)}$  label the respective coupling strengths of qubit- $j$  with the coupler and high-loss resonator, while  $g_{xy}$  describes the direct interaction between two qubits. The transmon coupler and high-loss resonator can respectively induce the coherent and non-Hermitian interactions between two qubits.

tonian  $H_{qc}^{(j)}$  are

$$\begin{aligned}
 H_0 &= \hbar\omega_a a^\dagger a + \sum_{j=1}^2 \frac{\hbar\omega_j}{2} \sigma_z^{(j)} + \frac{\hbar\omega_c}{2} \sigma_z^{(c)}, \\
 H_{xy} &= \hbar g_{xy} [\sigma_+^{(1)} \sigma_-^{(2)} + \sigma_+^{(2)} \sigma_-^{(1)}], \\
 H_{qc}^{(j)} &= \hbar g_j [\sigma_+^{(c)} \sigma_-^{(j)} + \sigma_+^{(j)} \sigma_-^{(c)}].
 \end{aligned} \tag{1}$$

The superscripts and subscripts  $j$  label the qubit-1 and qubit-2, respectively.  $\omega_j$ ,  $\omega_a$ , and  $\omega_c$  are the respectively transition frequency of qubit- $j$ , resonant frequency of resonator's fundamental mode, and transition frequency of coupler.  $a^\dagger$  and  $a$  are the photon creation and annihilation operators of resonator's fundamental mode, while  $\sigma_z^{(j)}$  ( $\sigma_z^{(c)}$ ) and  $\sigma_\pm^{(j)}$  ( $\sigma_\pm^{(c)}$ ) label the Pauli-Z and ladder operators of qubit- $j$  (coupler).  $g_{xy}$  labels the direct qubit-qubit coupling strength, and the interaction between resonator and transmon coupler is neglected.

By applying a detuned driving field on the superconducting

qubit, the amplitude and phase of resonator-qubit interaction can be tunable<sup>42-44</sup>. In this article, the qubits and resonator are in the dispersive coupling regimes, that is  $\lambda_j^{(0)} \ll |\Delta_{ja}|, |\Delta_{ja} + \alpha_j|$ , where  $\alpha_j$  is the anharmonicity of qubit- $j$ . After injecting a single tone microwave pulse with time-dependent amplitude  $\Omega_j(t)$  and phase  $\theta_j(t)$ , thus resonator-qubit- $j$  interaction becomes  $\lambda_j \exp(i\theta_j)$ <sup>42,43</sup>. Thus the Hamiltonian for amplitude and phase tunable resonator-qubit- $j$  interaction is

$$H_{qr}^{(j)} = \lambda_j [\exp(-i\theta_j) a^\dagger \sigma_-^{(j)} + \exp(i\theta_j) \sigma_+^{(j)} a], \tag{2}$$

where  $\lambda_j = (1/\sqrt{2})\lambda_j^{(0)}\alpha_j|\Omega_j|/[\Delta_{ja}(\Delta_{ja} + \alpha_j)]$ .  $\lambda_j^{(0)}$  is the bare coupling strength between the first-excited state of superconducting artificial atom- $j$  and the fundamental mode of resonator, and the corresponding frequency detuning is defined as  $\Delta_{ja} = \omega_j - \omega_a$ .

In the weak dispersive coupling regimes  $g_j/|\Delta_{jc}| \sim 1/3$  (with  $\Delta_{jc} = \omega_j - \omega_c$ ), the Schrieffer-Wolff transformation  $U = \exp \sum_{j=1}^2 (g_j/\Delta_{jc}) [\sigma_+^{(c)} \sigma_-^{(j)} - \sigma_+^{(j)} \sigma_-^{(c)}]$  can be applied to cancel the qubit-coupler interaction terms, thus the effective Hamiltonian becomes<sup>45,46</sup>

$$\begin{aligned}
 H' &= \hbar\omega_a a^\dagger a + \hbar \sum_{j=1}^2 \lambda_j \left[ \exp(-i\theta_j) a^\dagger \sigma_-^{(j)} + h.c. \right] \\
 &+ \hbar \left( \omega_j + \sum_{j=1}^2 \frac{g_j^2}{\Delta_{jc}} \right) \frac{\sigma_z^{(j)}}{2} + \hbar g_e \left[ \sigma_+^{(1)} \sigma_-^{(2)} + h.c. \right].
 \end{aligned} \tag{3}$$

$g_e = g_{xy} + g_1 g_2 / \Delta_e$  is the effective qubit-qubit coupling of coherent type, with  $2/\Delta_e = 1/\Delta_{1c} + 1/\Delta_{2c}$ .  $g_{xy}$  describes the direct qubit-qubit coupling strength, while  $g_1 g_2 / \Delta_e$  labels their indirect interaction induced by the transmon coupler<sup>47-50</sup>. The transmon coupler is dispersively coupled with the qubits and resonator and stays in the ground state in most of the time, after neglecting the free Hamiltonian the coupler usually functions as a tunable parameter of qubit-qubit coupling<sup>47</sup>. These approximations might neglect some processes of state leakages and crosstalks related to the coupler, but these errors can be significantly suppressed by the wave shape correction skill<sup>48</sup>. During the Schrieffer-Wolff transformation, there should be also corrected terms to qubit-resonator coupling that is proportional to  $(\lambda_j g_j / \Delta_j) \exp(i\theta_j) \sigma_z^{(j)} (a^\dagger \sigma_-^{(c)} + \sigma_+^{(c)} a)$  for the first-order correction. The resonator and coupler are not driven and they usually stay in the ground states, considering their weak coupling strength and large frequency detuning, so the corrections to  $H_{qr}^{(j)}$  are neglected in this article. Since  $g_{xy} \ll g_j$ , the invariance assumption is made for  $H_{xy}$  during the Schrieffer-Wolff transformation<sup>47</sup>.

In the rotating coordinates at resonator's frequency, the equations of motion for qubit- $j$  and photon in resonator are

$$\begin{aligned}
 \dot{a} &= -\gamma_a a - i \sum_{j=1}^2 \lambda_j \exp(-i\theta_j) \sigma_-^{(j)}, \\
 \dot{\sigma}_-^{(j)} &= - \left[ \frac{\gamma_j}{2} + i \left( \Delta_{ja} + \frac{g_j^2}{\Delta_{jc}} \right) \right] \sigma_-^{(j)} \\
 &- i \lambda_j \exp(i\theta_j) \sigma_z^{(j)} a - i g_e \sigma_z^{(j)} \sigma_-^{(j+1)},
 \end{aligned} \tag{4}$$

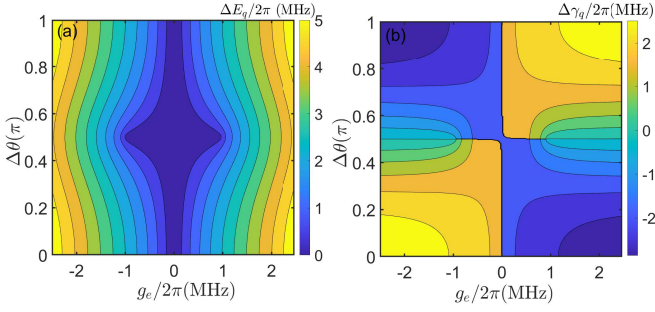


FIG. 2. (Color online) Differences in two eigenmodes' (a) energy levels ( $\Delta E_q$ ) and (b) damping rates ( $\Delta\gamma_q$ ) in the parameter space  $\{g_e, \Delta\theta\}$ . Both two qubits in the ground states:  $\langle\sigma_z^{(j)}\rangle = -1$ , with  $j = 1, 2$ . The other parameters:  $\omega_a/2\pi = 4.475$  GHz,  $\omega_1/2\pi = 4.5$  GHz,  $\omega_2/2\pi = 4.505$  GHz,  $\omega_c^{(max)}/2\pi = 5.20$  GHz,  $\gamma_1/2\pi = 1.00$  MHz,  $\gamma_2/2\pi = 1.01$  MHz,  $g_{xy}/2\pi = 4.0$  MHz,  $\lambda_{1,2}/2\pi = 11$  MHz,  $g_1/2\pi = 30$  MHz,  $g_2/2\pi = 30.3$  MHz, and  $\gamma_a/2\pi = 65$  MHz.

where  $\Delta_{ja} = \omega_j - \omega_a$ , and we assumed  $j+1 = 1$  for  $j = 2$ . In the case of  $\gamma_a \gg \gamma_j$ , with the adiabatic approximation, we can get  $a \approx -i \sum_{j=1}^2 \lambda_j \exp(-i\theta_j) \sigma_z^{(j)} / \gamma_a$ . Substituting it into the motion equation of  $\sigma_z^{(j)}$ , thus we get

$$\begin{aligned} \dot{\sigma}_-^{(j)} = & - \left[ \left( \frac{\gamma_j}{2} + \frac{\lambda_j^2 \sigma_z^{(j)}}{\gamma_a} \right) + i \left( \Delta_{ja} + \frac{g_j^2}{\Delta_{jc}} \right) \right] \sigma_-^{(j)} \\ & - \left[ ig_e + \frac{\lambda_j \lambda_{j+1} \exp[i(\theta_j - \theta_{j+1})]}{\gamma_a} \right] \sigma_z^{(j)} \sigma_-^{(j+1)}. \end{aligned} \quad (5)$$

Pauli-Z operator  $\sigma_z^{(j)}$  describes the population of qubit- $j$  and can be controlled by external driving fields. Though coupling to a high-loss resonator, the qubit' decoherence time should be much longer than the single qubit operation time, and the coherent time can be greatly enhanced by the tantalum-based superconducting devices<sup>51,52</sup>. The quantum states of qubits are controlled by the driving field, and the  $\langle\sigma_z^{(j)}\rangle$  can be considered as a transient stability value in the short period of experimental measurements. Thus the effective Hamiltonian for non-Hermitian superconducting circuit is

$$\frac{H_{non}}{\hbar} = \begin{pmatrix} \frac{1}{2}(\Delta'_{1a} - i\Gamma_1) & g_e - \frac{i\lambda_1\lambda_2 \exp(i\Delta\theta)}{\gamma_a} \\ g_e - \frac{i\lambda_1\lambda_2 \exp(-i\Delta\theta)}{\gamma_a} & \frac{1}{2}(\Delta'_{2a} - i\Gamma_2) \end{pmatrix}, \quad (6)$$

where  $\Delta\theta = \theta_1 - \theta_2$ ,  $\Delta'_{ja} = \Delta_{ja} + g_j^2/\Delta_{jc}$ , and  $\Gamma_j = \gamma_j + \lambda_j^2 \langle\sigma_z^{(j)}\rangle / \gamma_a$ . The eigenmodes of  $H_{non}$  are

$$\omega_{\pm} = \frac{\Delta'_{1a} + \Delta'_{2a}}{4} - i \frac{\Gamma_1 + \Gamma_2}{4} \pm \sqrt{R + iI}, \quad (7)$$

with

$$R = \frac{(\Delta'_{1a} - \Delta'_{2a})^2}{4} - \frac{(\Gamma_1 - \Gamma_2)^2}{4} + 4g_e^2 - \frac{4\lambda_1^2\lambda_2^2}{\gamma_a^2}, \quad (8)$$

$$I = -\frac{8g_e\lambda_1\lambda_2}{\gamma_a} \cos(\Delta\theta) - \frac{(\Gamma_1 - \Gamma_2)(\Delta'_{1a} - \Delta'_{2a})}{2}. \quad (9)$$

$Re(\omega_{\pm})$  and  $Im(\omega_{\pm})$  respectively describe the effective energy levels and damping rates of two eigenmodes.  $|R|$  and  $|I|$  decide separation distance between two energy levels, while  $\text{sgn}(R)$  and  $\text{sgn}(I)$  decide the level repulsions or attractions and relative size of damping rates.

In the article, the analytical and numerical calculations will adopt the experiment accessible parameters which have been widely used on the Xmon-based superconducting quantum chip<sup>53-56</sup>. The dispersive coupling between Transmon coupler and qubits is the mainstream solution to tune the qubit-qubit coupling<sup>47,48</sup>. The resonator can also function as a coupler to tune the coupling between two qubits, which has been theoretically and experimentally explored<sup>49,50,56,57</sup>. The high-loss resonator is an unusual device on superconducting quantum circuit which needs special design and fabrication techniques.

### III. CONTROLLABLE NON-HERMITIAN COUPLING

#### A. Energy level attraction and degeneracy

The complex energy spectrum of eigenmodes can be tuned by the phase and amplitude of resonator-qubit coupling, effective qubit-qubit coupling, and qubits' populations. In the case of  $R < 0$  and  $I = 0$ , the  $\sqrt{R + iI}$  becomes a pure imaginary number, thus the energy levels of two eigenmodes merge as one ( $\Delta E_q = 0$ ) and the EP can appear. Even for a small nonzero value of  $I$ , the energy levels of two eigenmodes can not overlap, and thus the EPs should be absent<sup>27</sup>.

The differences in energy levels or damping rates of two eigenmodes can be defined as  $\Delta E_q = Re(\omega_+) - Re(\omega_-) = 2Re(\sqrt{R + iI})$  or  $\Delta\gamma_q = Im(\omega_+) - Im(\omega_-) \approx 2Im(\sqrt{R + iI})$ , respectively. In the case of  $\langle\sigma_z^{(j)}\rangle = -1$  ( $\Gamma_1 - \Gamma_2 \neq 0$ ), the  $\Delta E_q$  and  $\Delta\gamma_q$  as the functions of  $g_e$  and  $\Delta\theta$  are plotted in Figs. 2(a) and 2(b), respectively. As shown in Fig. 2(a),  $\Delta E_q$  gets the local minimal values at deep blue color regimes. The local minimal values of  $\Delta\gamma_q$  locate at the regimes close to  $g_e/(2\pi) \approx \pm 1$  MHz and  $\Delta\theta \approx \pi/2$  as shown in Fig. 2(b). Thus EPs should be found close to the regimes of  $\Delta E_q \rightarrow 0$  and  $\Delta\gamma_q \rightarrow 0$  which corresponds to  $|g_e|/(2\pi) \approx \pm 1$  MHz and  $\Delta\theta \rightarrow \pi/2$ .

By setting two qubits in the ground states, the two eigenmodes' energy levels and damping rates as the function of coupling strength  $g_e$  are plotted in Figs. 3(a) and 3(b), respectively. Energy level attraction corresponds to the regimes of nearly degenerate energy levels coexisting with large separation for damping rates in Fig. 3. In order to see clearly, the pair of curves in blue and black colors are respectively moved by -0.5 MHz or 0.5 MHz parallel to the y-axis in Fig. 3(a). In the case of  $\Delta\theta = \pi/2$ , the first term in the right side of Eq. (9) is always zero, so there is no level degenerate point on pair of curves in blue color (see inset image) since  $\Delta'_{1a} - \Delta'_{2a} \neq 0$  in the parameter area of drawing. In the case of  $\Delta\theta \neq \pi/2$ , it is possible to satisfy  $I = 0$  as the variations of  $g_e$  (or  $\omega_c$ ), so the level degenerate points appear on the pairs of curves in red or black color. The scattering curves for damping rates of two eigenmodes are shown in Fig. 3(b), to see clearly the red and black colored curved are moved by 0.1 MHz and 0.2 MHz

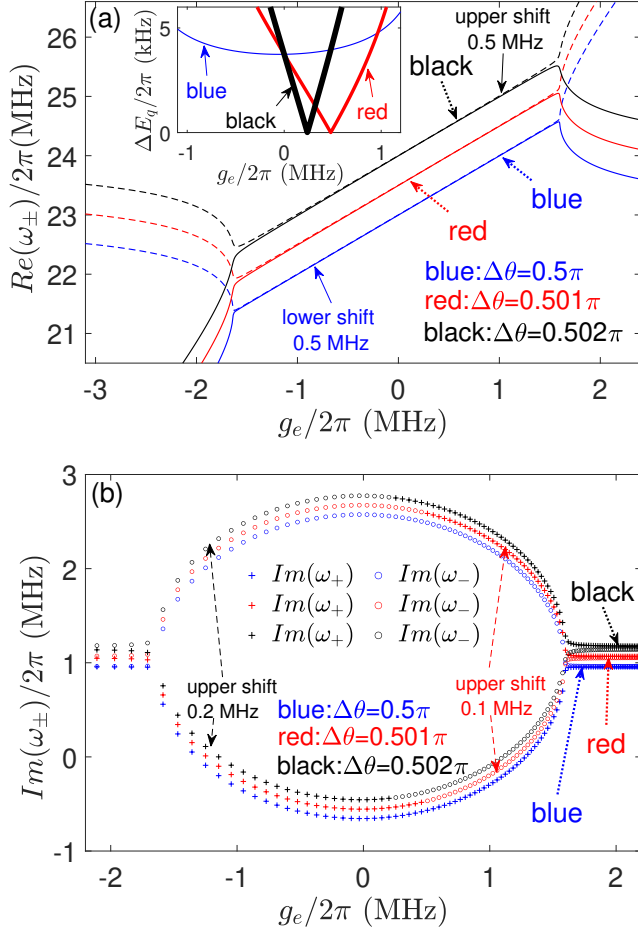


FIG. 3. (Color online) Energy level attraction. Eigenmodes' (a) energy levels  $Re(\omega_{\pm})$  and (b) damping rates  $Im(\omega_{\pm})$  as the function of  $g_e$ . The inset image show the energy level difference  $\Delta E_q$  of two Eigenmodes. Three pairs of colored curves in each figure for  $\Delta\theta = 0.5\pi$  (blue curves);  $0.501\pi$  (red curves); and  $0.502\pi$  (black curves). Both two qubits in the ground states:  $\langle\sigma_z^{(j)}\rangle = -1$ , with  $j = 1, 2$ .  $\lambda_1/2\pi = 11.3$  MHz,  $\lambda_2/2\pi = 11.6$  MHz, and the other parameters are the same as in Fig. 2.

parallel to the y-axis, respectively. On the pair of curves in red or black color, the eigenmodes' damping rates exchange with each other at the positions corresponding to level degenerate points in Fig. 3(a), so the energy level degenerate point should be an EP.

Figure 4(a) shows the variations of two eigenmodes' energy levels as the function of resonator-qubit coupling strength. For  $\Delta\theta = \pi/2$  and  $\Gamma_1 - \Gamma_2 = 0$ , the first and second terms in right side of Eq.(9) are always zeroes, so the energy level degeneracies appear for arbitrary values of  $\lambda_j$  in the energy level attraction regimes as shown by the blue, red, or green colors curves. If we tune the values of  $\lambda_j$  and  $\gamma_a$ , the positions of energy levels and EPs change for the pair of curves in green (and red) color (compared with the blue color curves). For  $\cos(\Delta\theta) = 0$ , in the case of  $\Delta'_{1a} - \Delta'_{2a} \neq 0$  (parameter area of drawing) and  $\Gamma_1 - \Gamma_2 \neq 0$ , thus the condition of  $I = 0$  can not be satisfied, so the energy level degeneracy does not appear on

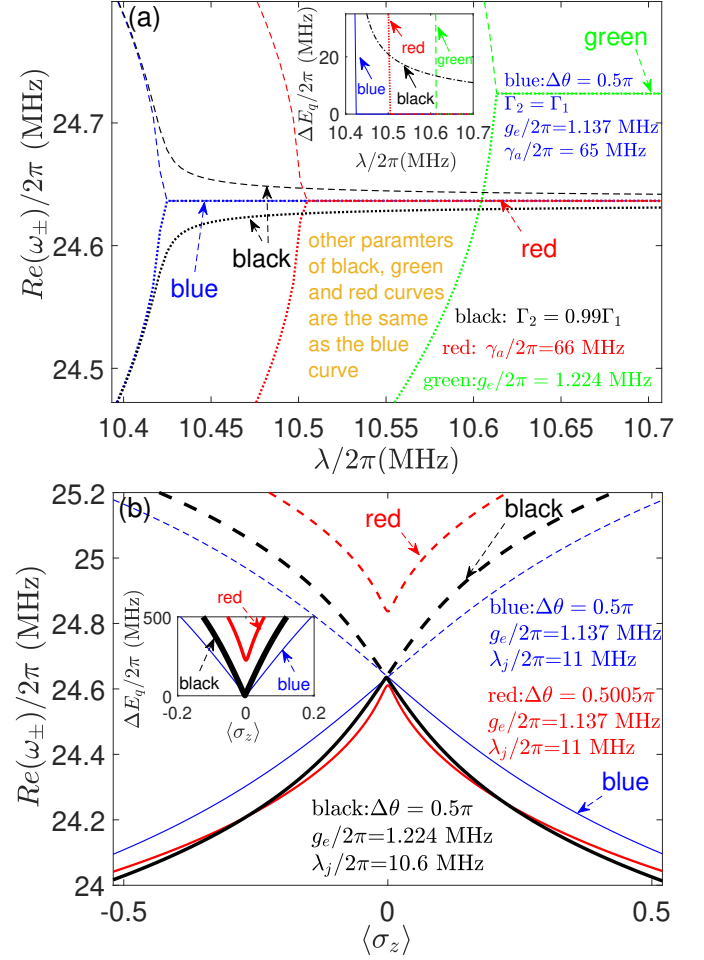


FIG. 4. (Color online) Controllable Energy levels and EPs. Controllable Energy levels and EPs.  $Re(\omega_{\pm})$  as the function of (a)  $\lambda$  (with  $\lambda = \lambda_1 = \lambda_2$ ) and (b)  $\langle\sigma_z\rangle$  (with  $\langle\sigma_z\rangle = \langle\sigma_z^{(1)}\rangle = -\langle\sigma_z^{(2)}\rangle$ ). The parameters for the pair of curves in blue color in (a) for:  $\Delta\theta = 0.500\pi$ ,  $\Gamma_2 = \Gamma_1$ ,  $g_e/2\pi = 1.137$  MHz, and  $\gamma_a/2\pi = 65$  MHz. Other curves take the same parameters of blue-colored curves except:  $g_e/2\pi = 1.224$  MHz for green-colored curves;  $\gamma_a/2\pi = 66$  MHz for red-colored curves, and  $\Gamma_2 = 0.99\Gamma_1$  for black-colored curves. The three pairs of colored curves in (b) for:  $\Delta\theta = 0.5\pi$ ,  $\lambda_j/2\pi = 11$  MHz, and  $g_e/2\pi = 1.137$  MHz (blue curves);  $\Delta\theta = 0.5005\pi$ ,  $\lambda_j/2\pi = 11$  MHz, and  $g_e/2\pi = 1.137$  MHz (red curves);  $\Delta\theta = 0.5\pi$ ,  $g_e/2\pi = 1.224$  MHz, and  $\lambda_j/2\pi = 10.6$  MHz (black curves). The inset figures in (a) and (b) label the corresponding level difference ( $\Delta E_q$ ). Two qubits are assumed in the ground states in (a), and the other parameters are the same as in Fig. 2.

the pair of curves in black color. The variations of two eigenmodes' energy levels as the function of qubits' populations are shown in Fig. 4(b). The energy level degeneracy appears on the pairs of curves in blue or black color (see inset image) at certain values of  $\langle\sigma_z^{(j)}\rangle$ , but there is no energy level degeneracy on the red color curves. To change the transient value of  $\langle\sigma_z^{(j)}\rangle$ , the qubit- $j$  should be firstly initialized to the ground states and then excited to the target quantum states.

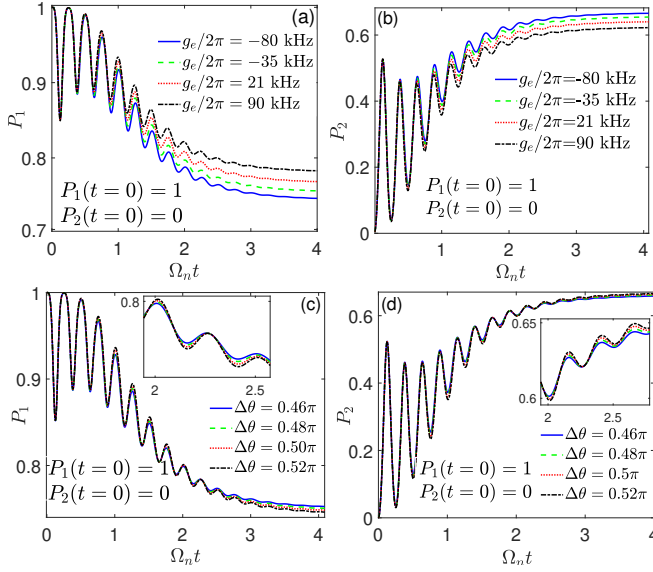


FIG. 5. (Color online) Controllable quantum state evolutions. The occupation probabilities of qubit-1 are shown in (a) and (c), while (b) and (d) describe the occupation probabilities of qubit-2. The four colored curves in (a) and (b) for different effective coupling strengths  $g_e/2\pi =$ : -80 kHz (blue-solid curves); -35 kHz (green-dashed curves); 21 kHz (red-dotted curves); 90 kHz (black-dash-dotted curves). The four colored curves in (c) and (d) for phase difference  $\Delta\theta =$ :  $0.46\pi$  (blue-solid curves);  $0.48\pi$  (green-dashed curves);  $0.50\pi$  (red-dotted curves);  $0.52\pi$  (black-dash-dotted curves). The  $\Delta\theta = 5\pi/12$  in (a) and (b), and  $g_e/2\pi = -31$  kHz in (c) and (d).  $\Omega_n = \lambda_1\lambda_2/\gamma_a$ ,  $\sigma_z^{(1)}(t=0) = 1$ ,  $\sigma_z^{(2)}(t=0) = -1$ , and the other parameters are the same as in Fig. 2.

## B. Controllable quantum state evolution

The changes of eigenmodes' energy levels and damping rates are quite significant around EPs, and the effects of EPs on the evolution of qubits' quantum states should be an interesting topic worth exploring. By disregarding the quantum jump terms, the time evolutions of qubits in non-Hermitian superconducting circuit can be calculated by the semiclassical master equation<sup>35,58,59</sup>

$$\dot{\rho} = -i(H_{non}\rho - \rho H_{non}^\dagger), \quad (10)$$

where  $\rho$  is the density operator of non-Hermitian circuit. Through the numerical calculations, the time evolution of qubits' quantum states can be obtained.

As indicated by Fig. 2, the EPs should appear close to the regimes of  $\Delta\theta \rightarrow \pi/2$  and  $g_e/(2\pi) \rightarrow \pm 1$  MHz. By preparing the qubit-1 in the excited state and qubit-2 in the ground state, the time evolution of occupation probabilities  $P_j$  ( $j=1,2$ ) are plotted in Figs. 5(a) and 5(b) (with  $\Omega_n = \lambda_1\lambda_2/\gamma_a$ ), respectively. The four curves correspond to different effective coupling strength  $g_e$ , and the nearly periodic oscillation on the curves indicate the energy exchanges between two qubits. The state exchange efficiency between two qubits becomes weaker close to EPs on the black dash-dotted curves, where the non-Hermitian interaction enhance the damping rates of

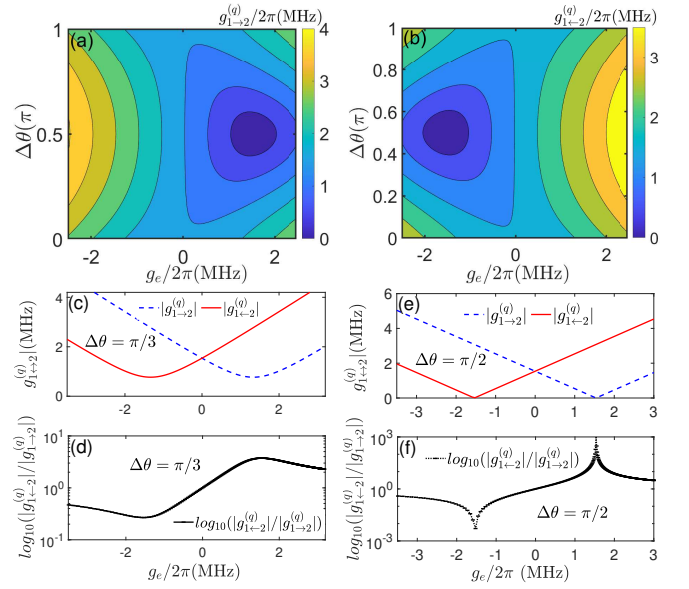


FIG. 6. (Color online) Nonreciprocal qubit-qubit coupling. Pseudocolor images of (a)  $g_{1\rightarrow 2}^{(q)}$  and (b)  $g_{1\leftarrow 2}^{(q)}$  in the parameter space  $\{\Delta\theta, g_e\}$ . One dimensional curves of  $g_{1\leftrightarrow 2}^{(q)}$  as the function of  $g_e$  for (c)  $\Delta\theta = \pi/2$  and (e)  $\Delta\theta = \pi/3$ , and corresponding non-reciprocal ratios  $|g_{1\rightarrow 2}^{(q)}|/|g_{1\leftarrow 2}^{(q)}|$  at (d)  $\Delta\theta = \pi/2$  and (f)  $\Delta\theta = \pi/3$ . The other parameters are:  $\omega_a/2\pi = 4.475$  GHz,  $\omega_1/2\pi = 4.5$  GHz,  $\omega_2/2\pi = 4.505$  GHz,  $\omega_c^{(max)}/2\pi = 5.20$  GHz,  $\gamma_1/2\pi = 1.00$  MHz,  $\gamma_2/2\pi = 1.01$  MHz,  $g_{xy}/2\pi = 4.0$  MHz,  $\lambda_{1,2}/2\pi = 11$  MHz,  $g_1/2\pi = 30$  MHz,  $g_2/2\pi = 30.3$  MHz,  $\gamma_a/2\pi = 65$  MHz, and  $\langle\sigma_z^{(j)}\rangle = -1$  (with  $j = 1, 2$ ).

two qubits. As the time evolves, the envelopes of curves for occupation probability  $P_1(t)$  ( $P_2(t)$ ) decrease (increase) to certain values.

The phase difference  $\Delta\theta$  also affects the qubits' occupation probabilities as shown in Figs. 5(c) and 5(d). The envelopes of  $P_1(t)$  ( $P_2(t)$ ) increase (decrease) at the beginning and finally stabilize at certain values. The variation of relative sizes between  $\sigma_z^{(1)}$  and  $\sigma_z^{(2)}$  can change the value and even sign of  $(\Gamma_1 - \Gamma_2)$  in Eqs. (8) and (9). This lead to the change for the sorts of colored curves, and thus the envelopes of four curves experience separation, polymerization, and they finally separate and stabilize at different values.

## IV. CONTROLLABLE NONRECIPROCAL COUPLING

Many studies have shown that the non-reciprocity can appear in the non-Hermitian systems<sup>60-65</sup>. In this section, we will explore the non-reciprocal coupling between two qubits in the superconducting circuit of Fig. 1. As indicated by Eq. (6), the bi-directional qubit-qubit coupling in non-Hermitian circuit can be defined as  $g_{1\rightarrow 2}^{(q)} = g_e - i\Omega_n \exp(\mp i\Delta\theta)$ , respectively. We can still get  $g_{1\rightarrow 2}^{(q)} \neq g_{1\leftarrow 2}^{(q)}$  in the case of  $\Delta\theta = n\pi$ . The local maximal (or minimal) values

of  $g_{1\rightarrow 2}^{(q)}$  and  $g_{1\leftarrow 2}^{(q)}$  don't overlap with each other in Figs. 6(a) and 6(b), which indicates the non-reciprocal coupling between two qubits<sup>63</sup>. One dimensional curves of  $g_{1\rightleftharpoons 2}^{(q)}$  as the function of coupling strength  $g_e$  are plotted in Figs. 6(c) ( $\Delta\theta = \pi/3$ ) and 6(e) ( $\Delta\theta = \pi/2$ ), and the corresponding curves of non-reciprocal ratio  $|g_{1\leftarrow 2}^{(q)}|/|g_{1\rightarrow 2}^{(q)}|$  are shown in Figs. 6(d) and 6(f), respectively. The different locations for local minimal (or maximal) values of  $g_{1\rightarrow 2}^{(q)}$  and  $g_{1\leftarrow 2}^{(q)}$  indicate the asymmetric qubit-qubit interactions, and the degree of non-reciprocity can be tuned by the phase difference  $\Delta\theta$ .

The non-reciprocal coupling might differentiate the time evolution processes of two identical qubits. By choosing the same transition frequencies, coupling strengths, damping rates, and initial states, the time evolution processes of two qubits can be calculated with the master equation in Eq.(10). For the initially excited states of two qubits, the difference in the occupation probabilities of two qubits are plotted in the parameter spaces of  $\{\Omega_n t, g_e\}$  in Fig. 7(a) and  $\{\Omega_n t, \Delta\theta\}$  in Fig. 7(b), respectively. The non-zero of  $(P_2 - P_1)$  in some regimes of Pseudo-color images in Fig. 7 reveal the asymmetry between the quantum state evolutions of non-reciprocal coupling qubits. The near periodic stripes of  $(P_2 - P_1)$  on Pseudo-color images indicate the different Rabi oscillation frequencies between two qubits, which can be easily measured with current low temperature measurement skills.

## V. CONCLUSION

The energy spectrum and quantum state evolutions are studied in non-Hermitian superconducting quantum circuit. The non-Hermitian and non-reciprocal interactions can be used to control the quantum state evolutions and state exchanges of two qubit, which might be useful for enhancing the fidelity of quantum gates and speeding up quantum state initialization on superconducting quantum chip. In this manuscript, we used mainstream parameters of current Xmon-based tunable coupling superconducting quantum chip which can be easily realized by current experiment skills. One main challenge is the high-loss superconducting resonator, but the fabrication of resonator with with the normal metal might be a promising choice.

## VI. ACKNOWLEDGMENT

We thank Zhiguang Yan for the useful discussions. H.W. is supported the Natural Science Foundation of Shandong Province under Grant No. ZR2023LZH002 and the Inspur artificial intelligence research institute. Y.-J.Z. is supported by National Natural Science Foundation under grant No. 62474012, Beijing Natural Science Foundation under grant No. 4222064, Scholarship from China Scholarship Council, Beijing Outstanding Young Scientist Program (JWZQ20240102009). X.-W.X. is supported by the National Natural Science Foundation of China (Grant Nos. 12064010 and 12247105), the Science and Technology Innovation Pro-

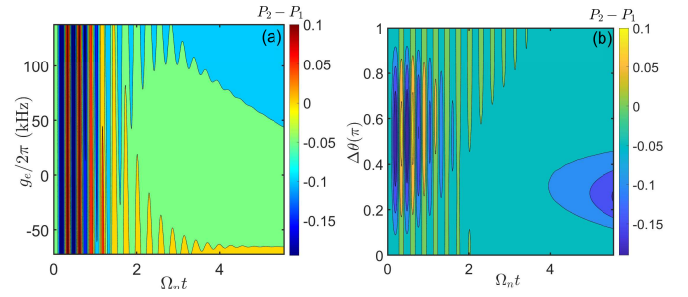


FIG. 7. (Color online) Asymmetric quantum state evolutions. Pseudo-color images for the difference in occupation probabilities  $(P_2 - P_1)$  in the parameter spaces (a)  $\{\Omega_n t, g_e\}$  and (b)  $\{\Omega_n t, \Delta\theta\}$ .  $\Delta\theta = \pi/2$  in (a) and  $g_e/2\pi = 5.3$  kHz in (b), and the other parameters are:  $\gamma_a/2\pi = 65$  MHz,  $g_{xy}/2\pi = 4.0$  MHz,  $\omega_j/2\pi = 4.5$  GHz,  $g_j/2\pi = 30$  MHz,  $\lambda_j/2\pi = 11$  MHz,  $\sigma_z^{(j)}(t=0) = 1$ , and  $\gamma_j/2\pi = 1$  MHz, with  $j = 1, 2$ .

gram of Hunan Province (Grant No. 2022RC1203), the Natural Science Foundation of Hunan Province of China (Grant No. 2021JJ20036), and the Hunan provincial major sci-tech program (Grant No. 2023ZJ1010).

- <sup>1</sup>C.M. Bender, S. Boettcher, and P.N. Meisinger, PT-symmetric quantum mechanics, *J. Math. Phys.* **40**, 2201 (1999).
- <sup>2</sup>C.M. Bender, D.C. Brody, and H.F. Jones, Complex extension of quantum mechanics, *Phys. Rev. Lett.* **89**, 270401 (2002).
- <sup>3</sup>G. Lévai and M. Znojil, Systematic search for PT -symmetric potentials with real energy spectra, *J. Phys. Math. Gen.* **33**, 7165 (2000).
- <sup>4</sup>C.M. Bender and S. Boettcher, Real Spectra in Non-Hermitian Hamiltonians Having PT Symmetry, *Phys. Rev. Lett.* **80**, 5243 (1998).
- <sup>5</sup>R. El-Ganainy, K.G. Makris, M. Khajavikhan, Z.H. Musslimani, S. Rotter, and D. N. Christodoulides, Non-Hermitian physics and PT symmetry, *Nat. Phys.* **14**, 11 (2018).
- <sup>6</sup>Ji Zou, Shu Zhang, and Yaroslav Tserkovnyak, Bell-state generation for spin qubits via dissipative coupling, *Phys. Rev. B* **106**, L180406 (2022).
- <sup>7</sup>Guo-Qiang Zhang, Wei Feng, Wei Xiong, Qi-Ping Su, and Chui-Ping Yang, Generation of long-lived  $W$  states via reservoir engineering in dissipatively coupled systems, *Phys. Rev. A* **107**, 012410 (2023).
- <sup>8</sup>Guo-Qiang Zhang, Wei Feng, Wei Xiong, Da Xu, Qi-Ping Su, and Chui-Ping Yang, Generating Bell states and  $N$ -partite  $W$  states of long-distance qubits in superconducting waveguide QED, *Phys. Rev. Applied* **20**, 044014 (2023).
- <sup>9</sup>Xin-You Lü, Hui Jing, Jin-Yong Ma, and Ying Wu, PT-Symmetry-Breaking Chaos in Optomechanics, *Phys. Rev. Lett.* **114**, 253601 (2015).
- <sup>10</sup>Weijian Chen, Ş.K. Özdemir, Guangming Zhao, J. Wiersig, and Lan Yang, Exceptional points enhance sensing in an optical microcavity, *Nature* **548**, 192 (2017).
- <sup>11</sup>Zhong-Peng Liu, Jing Zhang, Ş.K. Özdemir, Bo Peng, Hui Jing, Xin-You Lü, Chun-Wen Li, Lan Yang, F. Nori, and Yu-xi Liu, PT-Symmetric Cavities: Enhanced Sensitivity near the PT-Phase Transition, *Phys. Rev. Lett.* **117**, 110802 (2016).
- <sup>12</sup>Kai Zhang, Zhesen Yang, and Chen Fang, Universal non-Hermitian skin effect in two and higher dimensions, *Nat. Comm.* **13**, 2496 (2022).
- <sup>13</sup>Yaohua Li, Chao Liang, Chenyang Wang, Cuicui Lu, and Yong-Chun Liu, Gain-Loss-Induced Hybrid Skin-Topological Effect, *Phys. Rev. Lett.* **128**, 223903 (2022).
- <sup>14</sup>Guoqiang Xu, Xue Zhou, Ying Li, Qitao Cao, Weijin Chen, Yunfeng Xiao, Lan Yang, and Cheng-Wei Qiu, Non-Hermitian Chiral Heat Transport, *Phys. Rev. Lett.* **130**, 266303 (2023).
- <sup>15</sup>Liangyu Ding, Kaiye Shi, Qiuxin Zhang, Danna Shen, Xiang Zhang, and Wei Zhang, Experimental Determination of PT -Symmetric Exceptional Points in a Single Trapped Ion, *Phys. Rev. Lett* **126**, 083604 (2021).

- <sup>16</sup>Wei-Chen Wang, Yan-Li Zhou, Hui-Lai Zhang, Jie Zhang, Man-Chao Zhang, Yi Xie, Chun-Wang Wu, Ting Chen, Bao-Quan Ou, Wei Wu, Hui Jing, and Ping-Xing Chen, Observation of PT-symmetric quantum coherence in a single-ion system, *Phys. Rev. A* **103**, L020201 (2021).
- <sup>17</sup>B. Peng, S.K. Özdemir, F. Lei, F. Monifi, M. Gianfreda, G. L. Long, S. Fan, F. Nori, C. M. Bender, and L. Yang, Parity-timesymmetric whispering-gallery microcavities, *Nat. Phys.* **10**, 394 (2014).
- <sup>18</sup>L. Chang, X. Jiang, S. Hua, C. Yang, J. Wen, L. Jiang, G. Li, G. Wang, and M. Xiao, Parity-time symmetry and variable optical isolation in active-passive-coupled microresonators, *Nat. Photonics* **8**, 524 (2014).
- <sup>19</sup>L. Feng, Z. J. Wong, R.-M. Ma, Y. Wang, and X. Zhang, Single mode laser by parity-time symmetry breaking, *Science* **346**, 972 (2014).
- <sup>20</sup>H. Hodaei, M.-A. Miri, M. Heinrich, D.N. Christodoulides, and M. Khajavikhan, Parity-time-symmetric microring lasers, *Science* **346**, 975 (2014).
- <sup>21</sup>H. Hodaei, A.U. Hassan, S. Wittek, H. Garcia-Gracia, R. El-Ganainy, D. N. Christodoulides, and M. Khajavikhan, Enhanced sensitivity at higher-order exceptional points, *Nature (London)* **548**, 187 (2017).
- <sup>22</sup>A.A. Zyablovsky, A.P. Vinogradov, A.A. Pukhov, A.V. Dorofeenko, and A.A. Lisyansky, PT-symmetry in optics, *Phys. Usp.* **57**, 1063 (2014).
- <sup>23</sup>Huilai Zhang, Ran Huang, Sheng-Dian Zhang, Ying Li, Cheng-Wei Qiu, F. Nori, and Hui Jing, Breaking Anti-PT Symmetry by Spinning a Resonator, *Nano Lett.* **20**, 7594 (2020).
- <sup>24</sup>H. Xu, D. Mason, Luyao Jiang, and J.G.E. Harris, Topological energy transfer in an optomechanical system with exceptional points, *Nature* **537**, 80 (2016).
- <sup>25</sup>N. Wu, K. Cui, Q. Xu, X. Feng, F. Liu, W. Zhang, and Y. Huang, On-chip mechanical exceptional points based on an optomechanical zipper cavity, *Science Advances*, **9**, eabp8892 (2023).
- <sup>26</sup>Cheng Jiang, Yu-Long Liu, and M.A. Sillanpää, Energy-level attraction and heating-resistant cooling of mechanical resonators with exceptional points, *Phys. Rev. A* **104**, 013502 (2021).
- <sup>27</sup>N.R. Bernier, L.D. Tóth, A.K. Feofanov, and T.J. Kippenberg, Level attraction in a microwave optomechanical circuit, *Phys. Rev. A* **98**, 023841 (2018).
- <sup>28</sup>H. Liu, D. Sun, C. Zhang, M. Groesbeck, R. Mclaughlin, and Z.V. Vardeny, Observation of exceptional points in magnonic parity-time symmetry devices, *Sci. Adv.* **5**, eaax9144 (2019).
- <sup>29</sup>Xi-guang Wang, Lu-lu Zeng, Guang-hua Guo, and J. Berakdar, Floquet Engineering the Exceptional Points in Parity-Time-Symmetric Magnonics, *Phys. Rev. Lett.* **131**, 186705 (2023).
- <sup>30</sup>A.V. Sadovnikov, A.A. Zyablovsky, A.V. Dorofeenko, and S.A. Nikitov, Exceptional-Point Phase Transition in Coupled Magnonic Waveguides, *Phys. Rev. Applied* **18**, 024073 (2022).
- <sup>31</sup>Guo-Qiang Zhang, Shen Chen, Da Xu, N. Shammah, Meiyong Liao, Tie-Fu Li, Limin Tong, Shi-Yao Zhu, F. Nori, and J. Q. You, Exceptional Point and Cross-Relaxation Effect in a Hybrid Quantum System, *PRX Quantum* **2**, 020307 (2021).
- <sup>32</sup>M. Harder, Y. Yang, B.M. Yao, C.H. Yu, J.W. Rao, Y.S. Gui, R.L. Stamps, and C.-M. Hu, Level Attraction Due to Dissipative Magnon-Photon Coupling, *Phys. Rev. Lett.* **121**, 137203 (2018).
- <sup>33</sup>Yi Li, V. G. Yefremenko, M. Lisovenko, C. Trevillian, T. Polakovic, T. W. Cecil, P. S. Barry, J. Pearson, R. Divan, V. Tyberkevych, C. L. Chang, U. Welp, Wai-Kwong Kwok, and V. Novosad, Coherent Coupling of Two Remote Magnonic Resonators Mediated by Superconducting Circuits, *Phys. Rev. Lett.* **128**, 047701 (2022).
- <sup>34</sup>F.F. Sani, I.C. Rodrigues, D. Bothner, and G.A. Steele, Level attraction and idler resonance in a strongly driven Josephson cavity, *Phys. Rev. Research* **3**, 043111 (2021).
- <sup>35</sup>Weijian Chen, M. Abbasi, Y.N. Joglekar, and K.W. Murch, Quantum Jumps in the Non-Hermitian Dynamics of a Superconducting Qubit, *Phys. Rev. Lett.* **127**, 140504 (2021).
- <sup>36</sup>R. Navarathna, D.T. Le, A.R. Hamann, H.D. Nguyen, T.M. Stace, and A. Fedorov, Passive Superconducting Circulator on a Chip, *Phys. Rev. Lett.* **130**, 037001 (2023).
- <sup>37</sup>G.A. Starkov, M.V. Fistul, and I.M. Eremin, Schrieffer-Wolff transformation for non-Hermitian systems: Application for PT-symmetric circuit QED, *Phys. Rev. B* **108**, 235417 (2023).
- <sup>38</sup>F. Quijandría, U. Naether, S.K. Özdemir, F. Nori, and D. Zueco, PT-symmetric circuit QED, *Phys. Rev. A* **97**, 053846 (2018).
- <sup>39</sup>J.Q. You, Xuedong Hu, S. Ashhab, and F. Nori, Low-decoherence flux qubit, *Phys. Rev. B* **75**, 140515(R) (2007).
- <sup>40</sup>J. Koch, T.M. Yu, J. Gambetta, A.A. Houck, D.I. Schuster, J. Majer, A. Blais, M.H. Devoret, S.M. Girvin, and R.J. Schoelkopf, Charge-insensitive qubit design derived from the Cooper pair box, *Phys. Rev. A* **76**, 042319 (2007).
- <sup>41</sup>R. Barends, J. Kelly, A. Megrant, D. Sank, E. Jeffrey, Y. Chen, Y. Yin, B. Chiaro, J. Mutus, C. Neill, P. O'Malley, P. Roushan, J. Wenner, T.C. White, A.N. Cleland, and J.M. Martinis, Coherent Josephson Qubit Suitable for Scalable Quantum Integrated Circuits, *Phys. Rev. Lett.* **111**, 080502 (2013).
- <sup>42</sup>S. Zeytinoglu, M. Pechal, S. Berger, A.A. Abdumalikov, Jr., A. Wallraff, and S. Filipp, Microwave-induced amplitude- and phase-tunable qubit-resonator coupling in circuit quantum electrodynamics, *Phys. Rev. A* **91**, 043846 (2015).
- <sup>43</sup>M. Pechal, L. Huthmacher, C. Eichler, S. Zeytinoglu, A.A. Abdumalikov, Jr., S. Berger, A. Wallraff, and S. Filipp, Microwave-Controlled Generation of Shaped Single Photons in Circuit Quantum Electrodynamics, *Phys. Rev. X* **4**, 041010 (2014).
- <sup>44</sup>P. Magnard, P. Kurpiers, B. Royer, T. Walter, J.-C. Besse, S. Gasparinetti, M. Pechal, J. Heinsoo, S. Storz, A. Blais, and A. Wallraff, Fast and Unconditional All-Microwave Reset of a Superconducting Qubit, *Phys. Rev. Lett.* **121**, 060502 (2018).
- <sup>45</sup>S. Bravyi, D.P. DiVincenzo, and D. Loss, Schrieffer-wolff transformation for quantum many-body systems, *Annals of physics* **326**, 2793 (2011).
- <sup>46</sup>S. Richer, "Perturbative analysis of two-qubit gates on transmon qubits," Master's thesis, RWTH Aachen University (2013)..
- <sup>47</sup>F. Yan, P. Krantz, Y. Sung, M. Kjaergaard, D.L. Campbell, T. P. Orlando, S. Gustavsson, and W.D. Oliver, Tunable Coupling Scheme for Implementing High-Fidelity Two-qubit Gates, *Phys. Rev. Applied* **10**, 054062 (2018).
- <sup>48</sup>Y. Sung, L. Ding, J. Braumüller, A. Vepsäläinen, B. Kannan, M. Kjaergaard, A. Greene, G.O. Samach, C. McNally, D. Kim, A. Melville, B.M. Niedzielski, M.E. Schwartz, J.L. Yoder, T.P. Orlando, S. Gustavsson, and W.D. Oliver, Realization of High-Fidelity CZ and ZZ-Free iSWAP Gates with a Tunable Coupler, *Phys. Rev. X* **11**, 021058 (2021).
- <sup>49</sup>Hui Wang, Yan-Jun Zhao, Hui-Chen Sun, Xun-Wei Xu, Yong Li, Yarui Zheng, Qiang Liu, and Rengang Li, Controlling the qubit-qubit coupling in the superconducting circuit with double-resonator couplers, *Phys. Rev. A* **109**, 012601 (2024).
- <sup>50</sup>Hui Wang, Yan-Jun Zhao, Rui Wang, Xun-Wei Xu, Qiang Liu, Jianhua Wang, and Changxin Jin, Frequency adjustable resonator as a tunable coupler for Xmon qubits, *J. Phys. Soc. Jpn.* **91**, 104005 (2022).
- <sup>51</sup>A.P.M. Place, L.V.H. Rodgers, P. Mundada, B.M. Smitham, M. Fitzpatrick, Zhaoqi Leng, A. Premkumar, J. Bryon, A. Vrajitoarea, S. Sussman, Guangming Cheng, T. Madhavan, H.K. Babla, Xuan Hoang Le, Youqi Gang, B. Jäck, A. Gyenis, Nan Yao, R.J. Cava, N.P. de Leon, and A.A. Houck, New material platform for superconducting transmon qubits with coherence times exceeding 0.3 milliseconds, *Nat. Comm.* **12**, 1779 (2021).
- <sup>52</sup>Chenlu Wang, Xuegang Li, Huikai Xu, Zhiyuan Li, Junhua Wang, Zhen Yang, Zhenyu Mi, Xuehui Liang, Tang Su, Chuohong Yang, Guangyue Wang, Wenyang Wang, Yongchao Li, Mo Chen, Chengyao Li, Kehuan Linghu, Jiaxiu Han, Yingshan Zhang, Yulong Feng, Yu Song, Teng Ma, Jingning Zhang, Ruixia Wang, Peng Zhao, Weiyang Liu, Guangming Xue, Yirong Jin, and Haifeng Yu, Towards practical quantum computers: transmon qubit with a lifetime approaching 0.5 milliseconds, *npj Quan. Inf.* **8**, 3 (2022).
- <sup>53</sup>F. Arute, K. Arya, R. Babbush, D. Bacon, J. C. Bardin, R. Barends, R. Biswas, S. Boixo, F. G. S. L. Brandao, D. A. Buell, B. Burkett, Yu Chen, Zijun Chen, B. Chiaro, R. Collins, W. Courtney, A. Dunsworth, E. Farhi, B. Foxen, A. Fowler, C. Gidney, M. Giustina, R. Graff, K. Guerin, S. Habegger, M. P. Harrigan, M. J. Hartmann, A. Ho, M. Hoffmann, T. Huang, T. S. Humble, S. V. Isakov, E. Jeffrey, Zhang Jiang, D. Kafri, K. Kechedzhi, Julian Kelly, P. V. Klimov, S. Knysh, A. Korotkov, F. Kostritsa, D. Landhuis, M. Lindmark, E. Lucero, D. Lyakh, S. Mandr'a, J. R. McClean, M. McEwen, A. Megrant, Xiao Mi, K. Michielsen, M. Mohseni, J. Mutus, O. Naaman, M. Neeley, C. Neill, M. Y. Niu, E. Ostby, A. Petukhov, J. C. Platt, C. Quintana, E. G. Rieffel, P. Roushan, N. C. Rubin, D. Sank, K. J. Satzinger, V. Smelyanskiy, K. J. Sung, M. D. Trevithick, A. Vainsencher, B. Villalonga, T. White, Z. J. Yao, P. Yeh, A. Zalcman, H. Neven, J. M. Martinis, Quantum supremacy using a programmable superconducting processor, *Nature* **574**, 505 (2019).

- <sup>54</sup>Yulin Wu, Wan-Su Bao, Sirui Cao, Fusheng Chen, Ming-Cheng Chen, Xiawei Chen, Tung-Hsun Chung, Hui Deng, Yajie Du, Daojin Fan, Ming Gong, Cheng Guo, Chu Guo, Shaojun Guo, Lianchen Han, Linyin Hong, He-Liang Huang, Yong-Heng Huo, Liping Li, Na Li, Shaowei Li, Yuan Li, Futian Liang, Chun Lin, Jin Lin, Haoran Qian, Dan Qiao, Hao Rong, Hong Su, Lihua Sun, Liangyuan Wang, Shiyu Wang, Dachao Wu, Yu Xu, Kai Yan, Weifeng Yang, Yang Yang, Yangsen Ye, Jiangan Yin, Chong Ying, Jiale Yu, Chen Zha, Cha Zhang, Haibin Zhang, Kaili Zhang, Yiming Zhang, Han Zhao, Youwei Zhao, Liang Zhou, Qingling Zhu, Chao-Yang Lu, Cheng-Zhi Peng, Xiaobo Zhu, and Jian-Wei Pan, Strong Quantum Computational Advantage Using a Superconducting Quantum Processor, *Phys. Rev. Lett.* **127**, 180501 (2021).
- <sup>55</sup>Yunyan Yao, Liang Xiang, Zexian Guo, Zehang Bao, Yong-Feng Yang, Zixuan Song, Haohai Shi, Xuhao Zhu, Feitong Jin, Jiachen Chen, Shibo Xu, Zitian Zhu, Fanhao Shen, Ning Wang, Chuanyu Zhang, Yaozu Wu, Yiren Zou, Pengfei Zhang, Hekang Li, Zhen Wang, Chao Song, Chen Cheng, Rubem Mondaini, H. Wang, J. Q. You, Shi-Yao Zhu, Lei Ying, and Qiujiang Guo, Observation of many-body Fock space dynamics in two dimensions, *Nat. Phys.* **19**, 1459(2023).
- <sup>56</sup>Ming Gong, Shiyu Wang, Chen Zha, Ming-Cheng Chen, HeLiang Huang, Yulin Wu, Qingling Zhu, Youwei Zhao, Shaowei Li, Shaojun Guo, Haoran Qian, Yangsen Ye, Fusheng Chen, Chong Ying, Jiale Yu, Daojin Fan, Dachao Wu, Hong Su, Hui Deng, Hao Rong, Kaili Zhang, Sirui Cao, Jin Lin, Yu Xu, Lihua Sun, Cheng Guo, Na Li, Futian Liang, V. M. Bastidas, Kae Nemoto, W. J. Munro, Yong-Heng Huo, Chao-Yang Lu, Cheng-Zhi Peng, Xiaobo Zhu, Jian-Wei Pan, Quantum walks on a programmable two-dimensional 62-qubit superconducting processor, *Science* **372**, 948(2021).
- <sup>57</sup>Yulin Wu, Li-Ping Yang, Ming Gong, Yarui Zheng, Hui Deng, Zhiguang Yan, Yanjun Zhao, Keqiang Huang, Anthony D Castellano, William J Munro, Kae Nemoto, Dong-Ning Zheng, CP Sun, Yu-xi Liu, Xiaobo Zhu, Li Lu, An efficient and compact switch for quantum circuits, *npj Quan. Inf.* **4**, 50 (2018).
- <sup>58</sup>F. Roccati, G. Massimo Palma, F. Bagarello, and F. Ciccarello, Non-Hermitian physics and master equations, *Open Systems and Information Dynamics*, **29**, 2250004 (2022).
- <sup>59</sup>F. Minganti, A. Miranowicz, R.W. Chhajlany, and F. Nori, Quantum exceptional points of non-Hermitian Hamiltonians and Liouvillians: The effects of quantum jumps, *Phys. Rev. A* **100**, 062131 (2019).
- <sup>60</sup>Xun-Wei Xu, Yan-jun Zhao, Hui Wang, Ai-Xi Chen, and Yu-Xi Liu, Nonreciprocal transition between two nondegenerate energy levels, *Photon. Res.* **9**, 87 (2021).
- <sup>61</sup>Xun-Wei Xu, Yong Li, Baijun Li, Hui Jing, and Ai-Xi Chen, Nonreciprocity via Nonlinearity and Synthetic Magnetism, *Phys. Rev. Applied* **13**, 044070 (2020).
- <sup>62</sup>H. Ghaemi-Dizicheh, Transport effects in non-Hermitian nonreciprocal systems: General approach, *Phys. Rev. B* **107**, 125155 (2023).
- <sup>63</sup>X. Huang, C. Lu, C. Liang, H. Tao, and Y.-C. Liu, Loss induced nonreciprocity, *Light Sci. Appl.* **10**, 30 (2021).
- <sup>64</sup>F. Roccati, S. Lorenzo, G. Calajò, G.M. Palma, A. Carollo, and F. Ciccarello, Exotic interactions mediated by a non-Hermitian photonic bath, *Optica* **9**, 565 (2022).
- <sup>65</sup>F. Roccati, M. Bello, Zongping Gong, M. Ueda, F. Ciccarello, A. Chenu, and A. Carollo, F. Roccati, Hermitian and non-Hermitian topology from photon-mediated interactions, *Nat. Commun.* **15**, 2400 (2024).